PHYSICAL REVIEW B VOLUME 41, NUMBER 15 15 MAY 1990-II

Characterization of the electron gas in wide parabolic $GaAs/Al_xGa_{1-x}As$ quantum wells

E. G. Gwinn,* P. F. Hopkins, A. J. Rimberg, and R. M. Westervelt
Division of Applied Sciences and Department of Physics, Harvard University, Cambridge, Massachusetts 02138

M. Sundaram and A. C. Gossard
Department of Electrical and Computer Engineering and Materials Department, University of California, Santa Barbara, California 93106

(Received 2 January 1990)

We demonstrate the production of a thick layer of high-mobility electron gas by comparison of Shubnikov–de Haas oscillations with self-consistent calculations of the ground-state energy levels. Ion-gauge measurements of the average Al flux during a programmed growth sequence show that the Al profile for the parabolic-well structures studied here follows the design profile closely. The calculated and measured energy levels ($E_F - E_i$) agree within the uncertainty of the well parameters.

I. INTRODUCTION

Extensive studies of the two-dimensional electron gas have been carried out over the past 15 years, and have produced a good understanding of many of the properties of very-thin (10–100 Å) layers of high-mobility electrons.[1,2] Recently, remotely doped parabolic wells have been used to produce layers of high-mobility electron gas with much greater thickness (> 1000 Å) in the transitional range between two and three dimensions. The properties of this new type of electronic system remain relatively unexplored.[3–5]

Figures 1(a)–1(c) illustrate the process by which remotely doped parabolic wells can be used to produce a thick, uniform layer of electron gas. The empty parabolic well in Fig. 1(a) is created by varying the Al mole fraction x during growth to create a parabolic variation of the conduction-band edge $E_c(z)$ in the $Al_xGa_{1-x}As$ alloy. This parabolic potential is the same as the electrostatic potential of a spatially uniform slab of positive charge with density $n_+ = \epsilon K / 4\pi e^2$, where ϵ is the dielectric constant and $K = d^2E_c/dz^2$ is the curvature of the well. Electrons can be introduced into the well from remotely located donors, set back from both sides of the well, as shown in Fig. 1. In the Thomas-Fermi approximation these electrons act to screen the parabolic potential, and thus tend to form a spatially uniform slab with fixed three-dimensional density $n_{3D} \cong n_+$ and variable width w_e, as illustrated in Figs. 1(b) and 1(c). Because these electrons are spatially separated from the donor ions, their mobility can be quite large. The spatial uniformity of the electron gas in actual structures is an important issue, because the electron density $n_{3D}(z)$ is determined to a large extent by the local curvature of the well. Small deviations from parabolicity can produce sizable changes in the local electron density.

In this paper we present data for high-mobility samples which characterize parabolic well structures grown as fine superlattices by shuttering the Al source.[3] We have achieved a large low-temperature mobility $\mu = 2.3 \times 10^5$ $cm^2/V\,s$ for a layer of electron gas of width $w_e \cong 2000$ Å in a 4640-Å-wide parabolic well. We present evidence for good uniformity of the electron gas in this structure: (1) the computer-controlled shuttering sequence of the calibrated Al source produces an average Al flux profile that follows the design parabola to within ~6%, and (2) the subband energies from low-temperature Shubnikov–de Haas oscillation measurements agree within ~10% with theory for a parabolic well with the same sheet density. The effective three-dimensional density $n_+ = 7 \times 10^{15}$ cm^{-3} for this structure is below the density at which doped n-type GaAs becomes an insulator at low tempera-

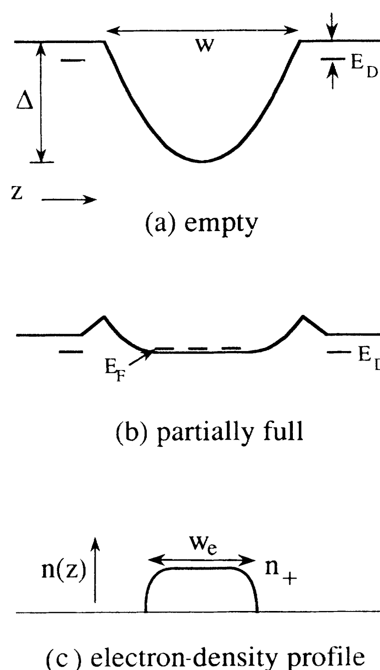

FIG. 1. Schematic illustration of the conduction-band edge in (a) an empty well, and (b) a partially full well. The electron-density profile in a partially filled well is shown in (c).

 ©1990 The American Physical Society

tures (the critical density[6] for the metal-insulator transition in n-type GaAs with shallow donors is $n_c \cong 1.5\times10^{16}$ cm^{-3}). We attribute this absence of freeze-out to the low donor density in the parabolic well channel, and note that the mobility exceeds the maximum mobility in uniformly doped n-type GaAs with the same carrier density by an order of magnitude.

II. THEORY

The energy of an electron in a parabolic well can be expressed as the sum of the kinetic energy for motion in the plane of the well, and a discrete energy level E_i in an effective potential along the growth direction. The energy levels E_i for an empty parabolic well are those of a simple harmonic oscillator (SHO), $E_1=(i-\frac{1}{2})\hbar\Omega$ for $i=1,2,3,\ldots,$ with frequency $\Omega=(K/m^*)^{1/2}$. Photoluminescence-excitation-spectroscopy measurements[7] on empty $GaAs/Al_xGa_{1-x}As$ parabolic wells, grown as fine superlattices, agree with this SHO spectrum, and have been used as a measure of the conduction-band offset $\Delta E_c/\Delta E_g$. It is of interest to note that the SHO frequency is simply equal to the plasma frequency corresponding to the design density n_+:$\Omega^2=\omega_p^2=4\pi n_+ e^2/\epsilon m^*$. For the wafer studied here, the SHO energy is $\hbar\Omega\approx3.3$ meV.

For a partially filled well, the total potential for a single electron is roughly the sum of the parabolic variation of the conduction-band edge and the electrostatic potential due to the other electrons, neglecting exchange and correlation terms. Thus the total self-consistent potential for a partially filled well has a flat bottom and steep walls. For this case, the energy levels E_i approach a square-well spectrum $E_i=(i^2/2m^*)(\pi\hbar/w_s)^2$, with the effective well width $w_s\sim w_e$. This energy-level structure has been confirmed in self-consistent solutions[8] to Schrödinger's and Poisson's equations including electron exchange and correlation terms.

Figure 2 shows the calculated electron-density profile for the parabolic well structure studied in this paper at $T=0$, for a sheet density $n_s=\int n(z)dz=1.40\times10^{11}$ cm^{-2}, chosen to match the measured low-temperature sheet density. The calculated energy levels E_i meV $=0.095i^2$ meV closely follow the expected square-well spacings for $w_s=w_e+393$ Å, where $w_e=n_s/n_+=2034$Å. As described in Ref. 8, many-body corrections[9] included in the calculation have a relatively small effect on the calculated energy levels, $<5\%$ for these parameters, but tend to enhance regions of high electron density somewhat.

The total electron-density profile $n(z)$ is shown in Fig. 2 along with the contributions $n_s^i|\phi_i(z)|^2$ from each subband, where $n_s^i=(m^*/\hbar^2\pi)(E_F-E_i)$ is the occupation, and $\phi_i(z)$ is the wave function. The total self-consistent potential is shown in Fig. 2 as the solid line. For the experimental sheet density $n_s=1.40\times10^{11}$ cm^{-2}, the electrons are predicted to occupy four subbands, adding so that the total density profile $n(z)$ in Fig. 2 is nearly constant over the width of the electron layer; the rms deviation of the calculated distribution from the design density

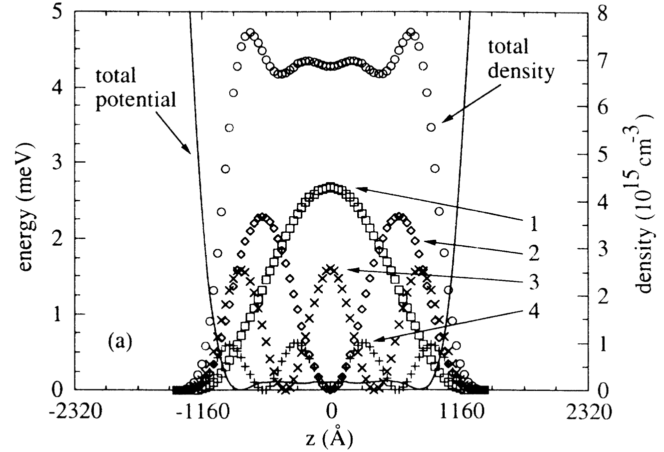

FIG. 2. Electron-density profile showing the total density with the contributions from each occupied subband, labeled 1–4, and the total self-consistent potential (solid line) as a function of position z in the well for a sheet density $n_s=1.4\times10^{11}$ cm^{-2}.

n_+ is $\sim12\%$. The calculated Fermi energy relative to the bottom of the lowest subband is $E_F-E_1=1.87$ meV, close to the value $E_F^{3D}=[\hbar^2(3\pi^2 n_+)^{2/3}]/2m^*=1.96$ meV for a three-dimensional electron gas of density n_+.

The primary uncertainties in the parameters used for these calculations are in the value of the conduction-band offset, taken to be $\Delta E_c/\Delta E_g=0.7$, for which $\Delta E_c/x=873$ meV, and the electron effective mass, taken to be a constant, $m^*=0.067m_0$. Reported values of the conduction-band offset vary by $\sim25\%$, with more recent measurements[10] approaching $\Delta E_c/\Delta E_g=0.7$. We have also neglected nonlinearity in the shift in conduction-band edge with Al mole fraction x. The effective mass in the well actually varies with Al mole fraction as $m^*/m_0=0.665+0.0835x$, which corresponds to a $\sim10\%$ change across the occupied region of the well, assuming symmetric filling. In addition, the subbands of the well have slightly different effective masses, because they average this mass variation differently.

Growth conditions are also important in the comparison of theory with experiment, even for perfectly parabolic wells. If the remotely located donor layers on opposite sides of the well deplete unequally, they add a linear term to the well potential, and shift the slab of electron gas away from center toward the more heavily depleted donor layer. To first order, such a shift has no effect on the electron profile $n(z)$, because the curvature of the well is unchanged. However, the average effective mass of the electron layer increases with shift Δz as $(\Delta z/w)^2$. Several factors in the molecular-beam-epitaxy- (MBE-) growth process can shift the electron layer off center, including asymmetries in donor diffusion, incorporation of deep compensating impurities, and self-compensation in the donor layers on opposite sides of the well. Unequal donor depletion from the surface and substrate interfaces can also lead to a shift (these differences are compensated for during growth, but are not accurately known). Due

to these factors, which are not taken into account in calculations, and due to the uncertainty in the conduction-band offset, agreement between experiment and theory at better than the 10% level is probably fortuitous.

III. SAMPLE CHARACTERISTICS

Parabolic well samples were produced[3] by varying the average Al mole fraction x in a fine superlattice of period 20 Å from $x=0$ at the center of the well to $x=0.3$ at the edges over a total width $w=4640$ Å, as illustrated in Fig. 1(a). This change in Al mole fraction corresponds to a well depth $\Delta E_c=262$ meV and design density $n_+=6.9\times10^{15}$ cm^{-3}, using $\Delta E_c/\Delta E_g=0.7$ for the conduction-band offset.[10] Electrons are introduced into the well from Si-donor layers symmetrically located on both sides of the well, and set back by 400-Å-thick undoped $Al_{0.3}Ga_{0.7}As$ buffer layers. For $x=0.3$ the Si-donor level is $\sim$90 meV below the conduction-band edge.[11]

Graded-gap MBE-grown structures such as parabolic wells have been made using two methods for controlling the Al fraction: the digital alloy technique based on shuttering the stabilized Al source,[3,4] and an analog technique based on changing the temperature of the Al source.[5,12] For the digital alloy technique, the composition alternates between GaAs and $Al_{x_0}Ga_{1-x_0}As$ in a fine 20-Å-period superlattice with x_0 fixed (here, $x_0=0.3$). The average Al mole fraction is smoothly varied by changing the time the Al shutter is open during the 20-Å period using computer control. The advantages of this technique are that the source temperatures are accurately stabilized and calibrated, and that the shutter timing can be controlled precisely. The primary disadvantage is that for small Al fractions near the center of the well the Al shutter is open a very short time, which is subject to error. To correct for the shutter response time in the present work, the actual shuttered Al flux is calibrated using an ion gauge at the same location as the substrate, and this calibration is used to correct the shutter opening times in order to produce a more nearly correct profile.

One might expect the presence of the superlattice in shuttered wells to have a large effect on electron motion inside the well. However, this is not the case, because the $Al_{0.3}Ga_{0.7}As$ superlattice barriers are sufficiently thin and low that the superlattice is nearly transparent to electrons, and does not significantly change the electron effective mass from its value in a continuously graded structure. A density-functional calculation of the energy levels including the superlattice potential accurately yields the same results as for continuous grading.[13,14] Optical[7] and resonant-tunneling[15] experiments on undoped parabolic wells have demonstrated the success of the digital alloy technique for accurate profile control. Note that for parabolic wells in magnetic fields the magnetic length $(\hbar c/eB)^{1/2}$ approaches the 20-Å superlattice period only for extremely large longitudinal magnetic fields $B\sim160$ T; at attainable fields the influence of the superlattice on magnetic phenomena is expected to be relatively small.

We chose to grow the parabolic wells by the digital alloy technique rather than by varying the temperature of the Al furnace, because of difficulty in achieving good control of the band edges with the latter method, even with computer control of the furnace temperature.[12] Band-gap-profile control via the Al furnace temperature is difficult because the time constants associated with changing the oven temperature are long, and the Al flux depends exponentially on the oven temperature. Near the bottom of a parabolic well with $x\cong0$, the temperature of the Al source must be changed rapidly, and is subject to error. In addition, significant thermal gradients are present in the source so that the temperature at the emitting surface is not the same as at the temperature sensor.

In order to test the accuracy of the shuttering program used to grow parabolic wells by the digital alloy technique, an ion gauge was placed at the location of the substrate in the MBE apparatus, and the Al flux was recorded during the computer-controlled shuttering program used to make parabolic wells. Figure 3(a) plots the measured average Al mole fraction x versus distance z for a 4640-Å-wide parabolic well. The dashed line shows the target parabolic profile and the solid line is the actual measured profile. Figure 3(b) shows the difference in mole fraction x between the measured and design profiles; the horizontal line corresponds to perfect agreement. As shown, the designed and measured profiles agree within $\Delta x=(+0.02, -0.01)$ across the entire well. The primary deviation shown in Fig. 3(a) takes the form of an increase in curvature of the parabola by approximately 12% above the design value over the central 2000 Å of the well. The error in the curvature of the well is largest in the center, where the time the Al shutter is open is very small. As described above, errors in curvature correspond to errors in density for electrons in the well. To estimate the magnitude of the curvature error, we numerically took the second derivative of Fig. 3(a). The largest deviations were two local maxima corresponding to a flattened region over the central $\sim$500 Å of the well. The

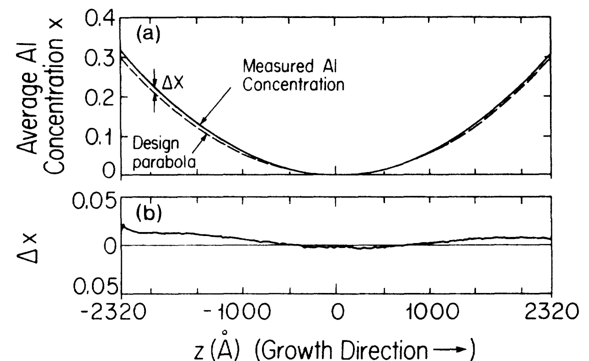

FIG. 3. (a) Design parabola and actual Al flux measured with an ion gauge at the substrate position expressed as Al mole fraction x vs depth z of the 4640-Å well for the computer-controlled shuttering program used to make the wafer studied in this paper. (b) The difference in Al mole fraction x between the measured and design profiles.

energy levels of empty wells seem fairly insensitive to comparable deviations from uniform curvature; photoluminescence-excitation spectra[7,16] of undoped wells grown by a similar shuttering program show the evenly spaced heavy- and light-hole transitions expected for a parabolic well. The effects of deviations in curvature on the density profile in partially filled wells will be discussed with the experimental results.

IV. MAGNETORESISTANCE AND HALL-EFFECT MEASUREMENTS

The data presented below were taken for two identically prepared samples from wafer MSPB24. Both were lithographically defined Hall bars with dimensions of 2.0×0.2 mm^2, with three potential probes on each side. Electrical contact to the electron layer was achieved by alloying In for ≈4 min at 400 °C. The samples were cooled in the dark in a He dilution refrigerator to $T\cong50$ mK, and transverse magnetoresistance (applied magnetic field perpendicular to the electron layer) and Hall-effect measurements were made using standard low-noise lock-in techniques, and the data were stored in a microcomputer. The power dissipated in the sample was kept very low (<0.05 pW) in order to avoid heating. The measured low-temperature, low-field ($B<0.1$ T) sheet density from Hall measurements is $n_H=1.41\times10^{11}$ cm^{-2}. Because different subbands can contribute disproportionately to n_H, the low-field Hall density is not necessarily a good measure of the true sheet density.[17] A more accurate measurement can be found from the periods of the low-field Shubnikov–de Haas oscillations in the transverse magnetoresistance data, as discussed below. As mentioned above, the measured low-field Hall mobility $\mu=2.3\times10^5$ cm^2/V s is quite high relative to uniformly doped GaAs with the same carrier concentration, evidence of the good quality of the samples.

Figure 4 is a plot of the low-field Hall resistance and Shubnikov–de Haas oscillations in the transverse magnetoresistance at $T=50$ mK. Oscillations are visible at $B\approx0.05$ T, and a complicated structure due to the interference of oscillations with different periods can be seen in the data. For a constant sheet density n_s, each subband produces an oscillation in resistance that is periodic in $1/B$, with frequency

$$\nu_i=\hbar S_i/2\pi e \ , \tag{1}$$

where $S_i=\pi k_{Fi}^2 = 2\pi m^*(E_F-E_i)/\hbar^2$ is the area of the corresponding electron orbits in k space, assuming isotropic, parabolic energy bands. At these low magnetic fields, spin splitting can be neglected. To measure the frequencies ν_i from different subbands, we took magnetoresistance data in the range $B=0-0.2$ T, filtered it with a digital low-pass filter, interpolated the data to be equally spaced in $1/B$, and then computed the fast Fourier transform (FFT) after applying a Hamming window. This procedure was repeated for three $T=50$ mK data sets taken for the same sample. The average of these spectra is shown in Fig. 5, which plots the logarithm of the power spectrum for the magnetoresistance versus oscillation frequency in $1/B$. The strong peaks in Fig. 5 fall at three frequencies $\nu_1=1.19$ T, $\nu_2=1.05$ T, and $\nu_3=0.60$ T. A fourth peak may occur near zero frequency, but is difficult to resolve from low-frequency noise. The sheet densities corresponding to each subband are given by $n_s^i=S_i/2\pi^2 =e\nu_i/\pi\hbar$, and are independent of the effective mass. Summing the contributions from the three observed subbands gives a total sheet density $n_s^{\text{tot}}=1.38\times10^{11}$ cm^{-2}. If a fourth subband were occupied, as predicted by theory, n_s^{tot} would increase by approximately 4%. Low-temperature capacitance-voltage profiles of different samples taken from the same wafer show three steps in the differential capacitance as the well is depleted, evidence for the occupation of a fourth subband.[18] The sheet density n_s can also be determined from the magnetic field positions of integer quantum-Hall-effect resistance minima for low filling factors; this yields $n_s=1.43\times10^{11}$ cm^{-2}, in excellent agreement with both the Shubnikov–de Haas oscillation and low-field Hall measurements above. For theoretical calculations of the wave functions and energy levels given above in Fig. 2, we used the value $n_s=1.40\times10^{11}$ cm^{-2}.

Table I presents a comparison of the experimentally

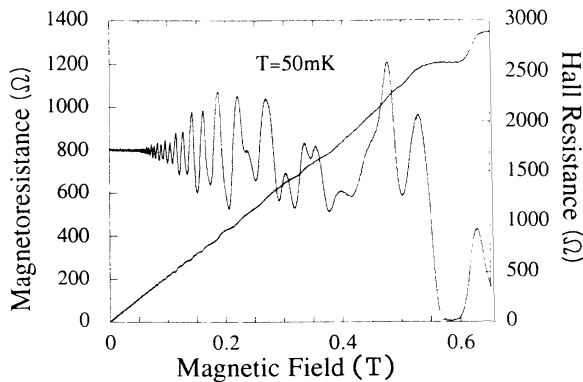

FIG. 4. Measured low-field magnetoresistance and Hall resistance at $T=50$ mK. Note the presence of Shubnikov–de Haas oscillations with multiple periods.

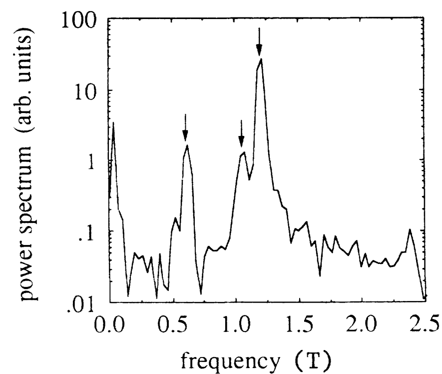

FIG. 5. Power spectrum for the low-field (0–0.2 T) magnetoresistance vs frequency in $1/B$; note the semilogarithmic scales. Three frequencies indicated by arrows can be clearly seen.

TABLE I. Comparison of the difference (in meV) between the Fermi energy E_F and the energy at the bottom of the ith subband, E_i, for experiment and theory for wafer MSPB24 with an electron sheet density $n_s = 1.4 \times 10^{11}$ cm^{-2}.

Energy	Experiment	Theory	Δ (%)
$E_F - E_1$	2.04	1.87	8
$E_F - E_2$	1.81	1.58	13
$E_F - E_3$	1.04	1.11	−7
$E_F - E_4$		0.44	

determined subband energies with theory. The only experimental input to the calculations is the measured sheet density n_s^{tot}; the other parameters are fixed at accepted values as described in Sec. II. As shown, the overall level of agreement between experiment and theory is at the 10% level for all three observed frequencies, good evidence that the wells are parabolic and their filling with electrons occurs according to the picture outlined in Sec. II. The absence of the fourth predicted subband from the Shubnikov–de Haas data is not surprising, because the number of electrons in this subband is predicted to be relatively small ($\sim$4% of the total), and the frequency is difficult to distinguish from low-frequency noise. The experimental structure at low frequencies from 0 to 0.1 T in Fig. 5 corresponds to an energy difference $E_F - E_4 = 0$–0.15 meV.

The two parameters in the theory which are the least well known are the conduction-band offset and the electron effective mass. The level of agreement shown in Table I is obtained by using an accepted value of the conduction-band offset $\Delta E_c / \Delta E_g = 0.7$ and the GaAs effective mass $m^* = 0.067 m_0$. As discussed above, the actual average effective mass is somewhat heavier, due to the thickness of the electron layer and a possible shift away from the center of the well. In fact, the level of agreement between theory and experiment in Table I is relatively insensitive to the assumed value of the effective mass. Because the experimental Shubnikov–de Haas oscillation periods directly measure areas in k space [Eq. (1)] independent of m^*, the energy differences shown in Table I vary with the assumed value m^* as $E_f - E_i \propto 1/m^*$. For theory, the same proportionality, $E_F - E_i \propto 1/m^*$, is also approximately true, because the subband energies E_i approximate those of a square well, $E_i \cong (i^2/2m^*)(\pi\hbar/w_s)^2$, and the density of states within each subband is $\propto m^*$. Thus comparison of Shubnikov–de Haas oscillation data with theory is not a sensitive way to determine the effective mass.

To estimate the effects of deviations from parabolicity, which can lead to nonuniformity in the density of the electron gas, we carried out self-consistent calculations for a truncated parabolic well with the same parameters as above, except for a 435-Å-wide flat spot on the bottom of the well. This well shape was chosen to model possible deviations from parabolicity suggested by Al flux-calibration data in Fig. 3. Such a flat region tends to produce a minimum in the electron density at the well center, as in a wide square well, because the mutual repulsion of the electrons is not compensated for by an attractive minimum in the well. These calculations show that the energy levels shift by $\sim$10% from their parabolic well values, with the same sign and magnitude as observed experimentally. The perturbation of the computed density takes the form of a minimum at the center of the well $\sim$50% below the design density n_+, flanked by two local maxima $\sim$20% above n_+. Although it is difficult to establish an exact correspondence between theory and the actual density profile, these calculations give an estimate of the magnitude and form of probable nonuniformities. By choosing the minimum Al fraction to be nonzero, and large enough for accurate control of the Al furnace shutter, we expect that the digital alloy technique will be able to produce even better agreement between the actual and design profiles, without sacrificing high mobility.

V. CONCLUSIONS

In conclusion, we have demonstrated the production of a thick, high-mobility layer of electron gas in a parabolic well grown by the digital alloy shuttering technique. Measurement of the Al flux during a computer-controlled growth sequence accurately follows a parabolic profile when the shutter opening times are calibrated to compensate for the shutter response time. Multiply-periodic Shubnikov–de Haas oscillations in the low-temperature magnetoresistance show that at least three subbands of the well are occupied and determine the subband energies relative to the Fermi energy. The experimental subband energies agree with self-consistent calculations of the energy levels to $\sim$10%, comparable to the uncertainty of the well parameters. The effects of small deviations from parabolicity are also discussed.

ACKNOWLEDGMENTS

This work was supported by the U.S. National Science Foundation at Harvard University under Grants No. DMR-88-17309 and No. DMR-86-14003, and at the University of California at Santa Barbara by the U.S. Air Force Office of Scientific Research under Grant No. AFOSR-88-0099.

*Present address: Department of Physics, University of California, Santa Barbara, Santa Barbara, CA 93106.

[1]R. E. Prange and S. M. Girvin, *The Quantum Hall Effect* (Springer-Verlag, New York, 1987).

[2]T. Ando, A. B. Fowler, and F. Stern, Rev. Mod. Phys. **54**, 437 (1982).

[3]M. Sundaram, A. C. Gossard, J. H. English and R. Westervelt, Superlatt. Microstruct. **4**, 683 (1988); M. Sundaram, A. C. Gossard, and J. H. English (unpublished).

[4]E. G. Gwinn, R. M. Westervelt, P. F. Hopkins, A. J. Rimberg,

M. Sundaram, and A. C. Gossard, Phys. Rev. B **39**, 6260 (1988).

[5]M. Shayegan, T. Sajoto, J. Jo, M. Santos, and H. D. Drew, Phys. Rev. B **40**, 3476 (1989).

[6]N. F. Mott and E. A. Davis, *Electronic Processes in Non-Crystalline Materials* (Oxford University Press, New York, 1989), p. 102.

[7]R. C. Miller, A. C. Gossard, D. A. Kleinman, and O. Munteau, Phys. Rev. B **29**, 3740 (1984).

[8]A. J. Rimberg and R. M. Westervelt, Phys. Rev. B **40**, 3970 (1989).

[9]See F. Stern and S. Das Sarma, Phys. Rev. B **30**, 840 (1984).

[10]See, for example, D. J. Wolford, T. F. Kuech, J. A. Bradley, M. A. Gell, D. Ninno, and M. Jaros, J. Vac. Sci. Technol. B **4**, 1043 (1986).

[11]E. F. Shubert and K. Ploog, Phys. Rev. B **30**, 7021 (1984).

[12]J. P. Harbison, L. D. Peterson, and J. Levkoff, J. Cryst. Growth **81**, 34 (1987).

[13]Yang Chu-liang and Yang Qing, Phys. Rev. B **37**, 1364 (1987).

[14]L. Brey, J. Dempsey, N. F. Johnson, and B. I. Halperin, Phys. Rev. B (to be published).

[15]S. Sen, F. Capasso, A. C. Gossard, R. A. Spah, A. L. Hutchinson, and S. N. G. Chu, Appl. Phys. Lett. **51**, 1428 (1987).

[16]J. H. Burnett, H. M. Cheong, W. Paul, P. F. Hopkins, E. G. Gwinn, A. J. Rimberg, R. M. Westervelt, M. Sundaram, and A. C. Gossard (unpublished).

[17]H. L. Stormer, A. C. Gossard, W. Wiegmann, Solid State Commun. **41**, 707 (1982).

[18]A. Wixforth, M. Sundaram, K. Ensslin, J. H. English, and A. C. Gossard, Appl. Phys. Lett. **56**, 454 (1990).